Inorganic Chemistry
Article

Inorg. Chem. **2009,** *48,* 4863–4872 **4863**
DOI:10.1021/ic900233d

Fluxionality in a Paramagnetic Seven-Coordinate Iron(II) Complex: A Variable-Temperature, Two-Dimensional NMR and DFT Study

David G. Lonnon, Graham E. Ball,* Ivan Taylor, Donald C. Craig, and Stephen B. Colbran*

School of Chemistry, University of New South Wales, Sydney, NSW 2052, Australia

Received February 4, 2009

The preparation and detailed characterizations of the high-spin seven-coordinate complexes $[M(\kappa^7N\text{-L})](ClO_4)_2$ (M = Mn (II), Fe(II); L = *N*,*N*,*N*′,*N*′-tetrakis(2-pyridylmethyl)-2,6-bis(aminomethyl)pyridine) are described. The X-ray crystal structures reveal seven-coordinate metal complex ions. Consideration of continuous shape measures reveals that the coordination environments about the metal ions are better described as having (C_s) face-capped trigonal prismatic symmetry than (C_2) pentagonal bipyramidal symmetry. The ($S = {}^5/_2$) Mn(II) species shows complicated X-band electron paramagnetic resonance (EPR) spectra and broad, unrevealing ^{1}H NMR spectra. In contrast, the ($S = 2$) Fe(II) complex is EPR-silent and shows completely interpretable ^{1}H NMR spectra containing the requisite number of paramagnetically shifted peaks in the range δ +150 to −60. The ^{13}C NMR spectra are likewise informative. Variable-temperature ^{1}H NMR spectra show coalescences and decoalescences indicative of an intramolecular process that pairwise-exchanges the nonequivalent pyridylmethyl "arms" of the two bis(pyridylmethyl)amine (bpa) domains. A suite of NMR techniques, including T_1 relaxation measurements and variable-temperature ^{1}H−^{1}H correlation spectroscopy, ^{1}H−^{1}H total correlation spectroscopy, ^{1}H−^{1}H nuclear Overhauser effect spectroscopy/exchange spectroscopy, and ^{1}H−^{13}C heteronuclear multiple-quantum coherence experiments, has been used to assign the NMR spectra and characterize the exchange process. Analysis of the data from these experiments yields the following thermodynamic parameters for the exchange: $\Delta H^{\ddagger} = 53.6 \pm 2.8$ kJ mol^{-1}, $\Delta S^{\ddagger} = -10.0 \pm 9.8$ J K^{-1} mol^{-1}, and $\Delta G^{\ddagger}$ (298 K) = 50.6 kJ mol^{-1}. Density functional theory (B3LYP) calculations have been used to explore the energetics of possible mechanistic pathways for the underlying fluxional process. The most plausible mechanism found involves dissociation of a pyridylmethyl arm to afford a strained six-coordinate species followed by rebinding of the arm in a different position to afford a new seven-coordinate transition state in which the pyridylmethyl arms within each bpa domain are essentially equivalent; the calculated energy barrier for this process is 53.5 kJ mol^{-1}, in good agreement with the observations.

Introduction

We have employed paramagnetic NMR spectroscopy to gain insights into the intramolecular ligand exchange processes within a seven-coordinate high-spin ($S = 2$) iron(II) complex. Seven-coordinate transition metal complexes remain relatively rare.[1] Such complexes typically adopt one of three geometries, either a face-capped trigonal antiprism (octahedron), a face-capped trigonal prism, or a pentagonal bipyramid. Experimental results and theory suggest that the energy difference between these alternatives is low. Thus, the actual geometry adopted is difficult to predict and, as much as anything, may be dictated by constraints imposed by the ligand(s). Investigations of intramolecular ligand exchange processes in such complexes are largely limited to diamagnetic organometallic complexes of the earlier second and third row elements, such as $M(CO)_2XL_4$ (M = Nb, Ta; X = (pseudo)halide, hydride, or alkyl; L = 2e$^-$ donor, e.g., PR_3), $M(CO)_3XL_3$ (M = Nb, Ta), and $M(CO)_3X_2L_2$ (M = Mo, W) systems, studied by "conventional" NMR spectroscopy.[1−13]

*To whom correspondence should be addressed. E-mail: g.ball@unsw.edu.au (G.E.B.); s.colbran@unsw.edu.au (S.B.C.).

(1) Casanova, D.; Alemany, P.; Bofill, J. M.; Alvarez, S. *Chem. Eur. J.* **2003**, *9*, 1281–1295.
(2) Baker, P. K. *Chem. Soc. Rev.* **1998**, *27*, 125–131.
(3) Baker, P. K.; Beckett, M. A.; Severs, L. M. *J. Organomet. Chem.* **1991**, *409*, 213–217.
(4) Brisdon, B. J.; Cartwright, M.; Hodson, A. G. W.; Mahon, M. F.; Molloy, K. C. *J. Organomet. Chem.* **1992**, *435*, 319–35.
(5) Carnahan, E. M.; Rardin, R. L.; Bott, S. G.; Lippard, S. J. *Inorg. Chem.* **1992**, *31*, 5193–5201.
(6) Saadeh, C.; Colbran, S. B.; Craig, D. C.; Rae, A. D. *Organometallics* **1993**, *12*, 133–9.
(7) Carlton, L.; Davidson, J. L.; Vasapollo, G.; Douglas, G.; Muir, K. W. *J. Chem. Soc., Dalton Trans.* **1993**, 3341–3347.
(8) Baker, P. K.; Muldoon, D. J.; Hursthouse, M. B.; Coles, S. J.; Lavery, A. J.; Shawcross, A. *Z. Naturforsch., B: Chem. Sci.* **1996**, *51*, 263–266.
(9) Chisholm, M. H.; Folting, K.; Kramer, K. S.; Streib, W. E. *J. Am. Chem. Soc.* **1997**, *119*, 5528–5539.
(10) Young, C. G.; Thomas, S.; Gable, R. W. *Inorg. Chem.* **1998**, *37*, 1299–1306.
(11) Sommer, R.; Lonnecke, P.; Reinhold, J.; Baker, P. K.; Hey-Hawkins, E. *Organometallics* **2005**, *24*, 5256–5266.
(12) Jackson, A. B.; White, P. S.; Templeton, J. L. *Inorg. Chem.* **2006**, *45*, 6205–6213.
(13) Gusev, D. G.; Hubener, R.; Burger, P.; Orama, O.; Berke, H. *J. Am. Chem. Soc.* **1997**, *119*, 3716–3731.

© 2009 American Chemical Society
Published on Web 4/28/2009

While relatively rare, seven-coordinate complexes of first-row transition metals are nevertheless well-established.[14−26] However, we are unaware of any studies of intramolecular ligand exchange within these complexes. This is largely because the complexes are high-spin and paramagnetic; thus, "conventional wisdom" deems the exchange processes to be intractable by NMR spectroscopic investigation. In this report, we show that NMR spectroscopy may still be useful in the study of ligand exchange. Specifically, exchange of the pyridylmethyl "arms" in the all-*N*-donor, high-spin ($S = 2$) iron(II) system, $[Fe(\kappa^7N\text{-L})]^{2+}$ (L = tetrakis(2-pyridylmethyl)-2,6-bis(aminomethyl)pyridine), has been characterized in detail by NMR experiments, and a plausible mechanism for the fluxional process is proposed on the basis of DFT calculations. The manganese(II) congener, $[Mn(\kappa^7N\text{-L})]^{2+}$, is also described.[27] The results are contrasted with the recent findings of Töftlund and co-workers for the exchange of a dangling, noncoordinated 2-pyridylmethyl "arm" and the coordinated 2-pyridylmethyl donors within the diamagnetic low-spin, distorted octahedral complex ion, $[Ru(\kappa^6N\text{-L})]^{2+}$.[28]

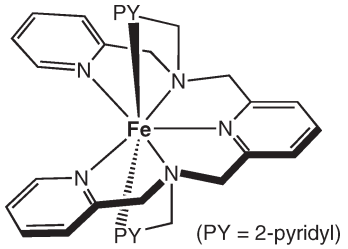

$[Fe(L)]^{2+}$

Results and Discussion

Syntheses. We previously reported the synthesis and the solution and solid-state properties of a range of five-coordinate copper(II) dimers spanned by L.[29,30] This work revealed L to be a useful binucleating ligand. Töftlund and co-workers' recent description of $[Ru(\kappa^6N\text{-L})]^{2+}$ reveals that L can support octahedral coordination, albeit with considerable geometric strain and distortion.[28] Further evidence of the versatility of L comes from this work: crystals of pale-pink $[Mn(\kappa^7N\text{-L})][ClO_4]_2$ and clear-yellow $[Fe(\kappa^7N\text{-L})][ClO_4]_2$ were directly obtained upon mixing L and the respective metal perchlorate salt in alcoholic media.

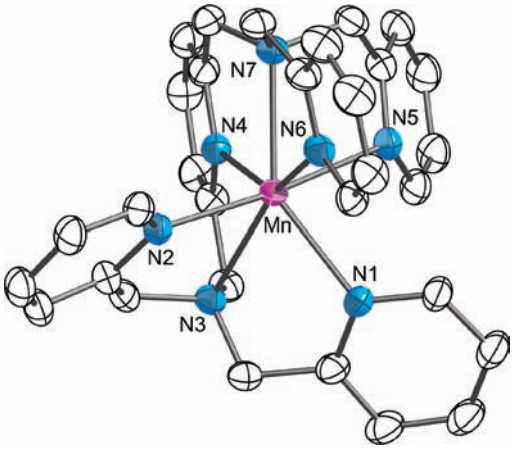

Figure 1. View of the $[Mn(L)]^{2+}$ cation, from the X-ray crystal structure of $[Mn(L)](ClO_4)_2$, which is isostructural with the $[Fe(L)]^{2+}$ cation (for clarity, 40% thermal ellipsoids and non-H atoms only are shown).

X-Ray Crystallography. The solid-state structures of $[Mn(L)](ClO_4)_2$ and $[Fe(L)](ClO_4)_2$ comprise discrete $[M(L)]^{2+}$ (M = Mn(II), Fe(II)) and perchlorate ions. The $[M(L)]^{2+}$ ions are isostructural, Figure 1, and chiral as L wraps in either a left- or right-handed fashion about the metal ion, and each unit cell comprises the two enantiomers plus counterions. The Mn−N and Fe−N bond distances, Table 1, are indicative of high-spin manganese(II) (d^5) and high-spin iron(II) (d^6) centers. The longest Mn−N distance is Mn−N5, 2.546(3) Å. The shortest is Mn−N4, 2.267(3) Å, and the others are 2.306−2.396 Å. The Fe−N distances are overall slightly shorter, with the longest Fe−N distance being Fe−N5, 2.539(3) Å, the shortest being Fe−N4, 2.167(3) Å, and the others being 2.219−2.347 Å. In each case, the unique, longer M(II)−N5 distance is substantially shorter than the sum of the van der Waal's radii of the metal ion and nitrogen (at ∼2.8 Å for a first-row transition metal ion) and thus is properly considered "bonding".[26]

The NMR spectra of the $[Fe(L)]^{2+}$ cation reveal that it has C_2 symmetry in solution, consistent with a pentagonal bipyramidal geometry in which one pyridylmethyl "arm" of each bis(pyridylmethyl)amine (bpa) domain adopts an equatorial position and the other an axial position (see below). In such a description, N2 and N5 are the axial donors (see Figures 1 and 2 and Figure 1S, Supporting Information), and the N2−M−N5 angles about the metal centers are 172.5(1)° (M = Mn) and 172.8(1)° (M = Fe). The sum of the adjacent N−M−N angles within the pentagonal plane are 375° (M = Mn) and 377° (M = Fe). The deviation from 360° reflects some puckering of the pentagonal

(14) Mizuta, T.; Wang, J.; Miyoshi, K. *Inorg. Chim. Acta* **1995**, *230*, 119–25.
(15) Che, C.-M.; Chang, C.-W.; Yang, S.-M.; Guo, C.-X.; Lee, C.-Y.; Peng, S.-M. *J. Chem. Soc., Dalton Trans.* **1995**, 2961–6.
(16) Allen, C. S.; Chuang, C.-L.; Cornebise, M.; Canary, J. W. *Inorg. Chim. Acta* **1995**, *239*, 29–37.
(17) Drew, M. G. B.; Othman, A. H. B.; McFall, S. G.; McIlroy, P. D. A.; Nelson, S. M. *J. Chem. Soc., Dalton Trans.* **1977**, 1173–80.
(18) Dees, A; Zahl, A.; Puchta, R.; van Eikema Hommes, N. J. R.; Heinemann, F. W.; Ivanovi-Burmazovi, I. *Inorg. Chem.* **2007**, *46*, 2459–2470.
(19) Deroche, A.; Morgensternbadarau, I.; Cesario, M.; Guilhem, J.; Keita, B.; Nadjo, L.; Houeelevin, C. *J. Am. Chem. Soc.* **1996**, *118*, 4567–4573.
(20) Lah, M. S.; Chun, H. *Inorg. Chem.* **1997**, *36*, 1782–1785.
(21) Oki, A. R.; Gogineni, P.; Yurchenko, M.; Young, V. G.Jr. *Inorg. Chim. Acta* **1997**, *257*, 279–283.
(22) Atwood, J. L.; Junk, P. C. *Polyhedron* **2000**, *19*, 85–91.
(23) Bu, X.-H.; Chen, W.; Zhang, Z.-H.; Zhang, R.-H.; Kuang, S.-M.; Clifford, T. *Inorg. Chim. Acta* **2000**, *310*, 110–114.
(24) Morgenstern-Badarau, I.; Lambert, F.; Renault, J. P.; Cesario, M.; Marechal, J. D.; Maseras, F. *Inorg. Chim. Acta* **2000**, *297*, 338–350.
(25) Baldeau, S. M.; Slinn, C. H.; Krebs, B.; Rompel, A. *Inorg. Chim. Acta* **2004**, *357*, 3295–3303.
(26) For a discussion of the distance criteria for high-spin Mn(II)−N and high-spin Fe(II)−N bonds in six- and seven-coordinate complexes, see: Brewer, C.; Brewer, G.; Butcher, R. J.; Carpenter, E. E.; Cuenca, L.; Noll, B. C.; Scheidt, W. R.; Viragh, C.; Zavalij, P. Y.; Zielaskia, D. *Dalton Trans.* **2006**, 1009–1019.
(27) The structure of $[Mn(\kappa_7N\text{-L})](ClO_4)_2 \cdot 0.435H_2O$ is described in a recent crystal structure report: Hazell, A.; Toftlund, H. Acta Crystallogr. 2007, E63, m328–m329.
(28) Akermark, B.; Bjernemose, J.; Borje, A.; Chmielewski, P. J.; Paulsen, H.; Simonsen, O.; Stein, P. C.; Toftlund, H.; Wolny, J. A. *Dalton Trans.* **2004**, 1215–1220.
(29) Lonnon, D. G.; Craig, D. C.; Colbran, S. B.; Bernhardt, P. V. *Dalton Trans.* **2004**, 778–787.
(30) Lonnon, D. G.; Craig, D. C.; Colbran, S. B. *Inorg. Chem. Commun.* **2002**, *5*, 958–962.

Table 1. Key Bond Length and Bond Angle Data from the X-Ray Crystal Structures of $[M(L)](ClO_4)_2$ (M = Mn, Fe)

bond lengths (Å)					
	Mn	Fe		Mn	Fe
M−N1	2.310(3)	2.219(3)	M−N5	2.546(3)	2.539(3)
M−N2	2.337(3)	2.331(3)	M−N6	2.306(3)	2.261(3)
M−N3	2.396(3)	2.347(3)	M−N7	2.387(3)	2.326(3)
M−N4	2.267(3)	2.167(3)			
bond angles (deg)					
	Mn	Fe		Mn	Fe
N1−M−N2	107.3(1)	109.5(1)	N3−M−N4	68.3(1)	71.0(1)
N1−M−N3	71.9(1)	72.5(1)	N3−M−N5	106.4(1)	108.6(1)
N1−M−N4	121.7(1)	122.5(1)	N3−M−N6	145.0(1)	139.9(1)
N1−M−N5	78.3(1)	77.5(1)	N3−M−N7	138.6(1)	143.5(1)
N1−M−N6	91.4(1)	87.0(1)	N4−M−N5	74.1(1)	74.0(1)
N1−M−N7	142.5(1)	138.7(1)	N4−M−N6	143.0(1)	146.1(1)
N2−M−N3	71.6(1)	72.6(1)	N4−M−N7	71.8(1)	74.3(1)
N2−M−N4	98.6(1)	100.0(1)	N5−M−N6	99.7(1)	99.7(1)
N2−M−N5	172.5(1)	172.8(1)	N5−M−N7	72.3(1)	71.6(1)
N2−M−N6	85.2(1)	82.9(1)	N6−M−N7	71.6(1)	72.2(1)
N2−M−N7	104.3(1)	103.1(1)			

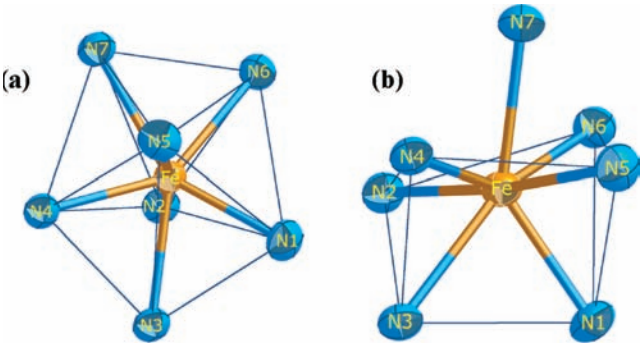

Figure 2. Views of the X-ray crystal structure of $[Fe(L)]^{2+}$ (with 40% thermal ellipsoids for the Fe- and N-donor atoms only shown) emphasizing alternative descriptions of the coordination geometry as (a) pentagonal bipyramidal and (b) face-capped trigonal prismatic (see text).

plane to minimize steric interactions between the terminal pyridyl donors: N1−M−N6 is more open at 91.4(1)° (M = Mn) and 87.0(1)° (M = Fe) than the other N−M−N angles for adjacent donors, which are all close to the expected 72°.

An analysis of the solid-state structures of the complex ions using continuous shape measures,[1,31,32] however, is revealing. It shows that the $[M(L)]^{2+}$ complex cations are actually closer to a face-capped trigonal prismatic geometry (shape measures are 2.7 and 2.1 for Mn and Fe, respectively) than to a pentagonal bipyramidal geometry (shape measures are 3.9 and 3.2). In the face-capped trigonal prismatic description of the structures, the N7 amine adopts the axial position. Figure 2 and Figure S1 (Supporting Information) illustrate these alternative coordination geometry descriptions for the $[Fe(L)]^{2+}$ cation.

Electronic Spectroscopy. The UV−vis−NIR spectrum of $[Mn(L)][ClO_4]_2$ is devoid of peaks with extinction coefficients greater than 1 M^{-1} cm^{-1}, consistent with a high-spin d^5 manganese(II) complex. In contrast, $[Fe(L)][ClO_4]_2$ shows a strong band at 400 nm in the solid state and at ~395 nm (~1000 M^{-1} cm^{-1}) in a range of organic solvents (Figure S2, Supporting Information), which is attributed to Fe(II)-to-pyridyl donor charge transfer transitions on the basis of previously assigned spectra of analogous high-spin iron(II) complexes. The spectrum of the iron complex also shows a weak band at ~1160 nm (~10 M^{-1} cm^{-1}). The yellow color of $[Fe(L)][ClO_4]_2$ is unchanged at 77 K (immersion in liquid nitrogen), indicative of the absence of a spin transition[33] down to this temperature.

Cyclic Voltammetry. $[Mn(L)][ClO_4]_2$ is inactive from +1.5 to −1.5 V (potentials against the ferrocenium/ferrocene couple). Over the same potential range, $[Fe(L)][ClO_4]_2$ shows a quasi-reversible Fe(II)/Fe(III) couple at +0.51 V (at 100 mV s^{-1} scan rate, ΔE_p = 140 mV, cf. 65 mV for the ferrocenium/ferrocene couple). No other processes are observed. The slow electron transfer kinetics may reflect a structural change, for example, to six-coordination, concurrent with the Fe(II)/Fe(III) couple.

Electron Paramagnetic Resonance (EPR) Spectroscopy. The complicated X-band EPR spectra of $[Mn(L)][ClO_4]_2$ at 77 K both in the solid state and in frozen dichloromethane, acetonitrile, or dimethylformamide solution (Figure S3, Supporting Information) are typical for monomeric manganese(II) systems and correspond to the superposition of the subspectra for the various excited spin states (S = 1−5).[34] An X-band EPR signal from high-spin iron(II) (S = 2 ground state) is usually inaccessible,[35] and as expected, no EPR signal was observed for $[Fe(L)](ClO_4)_2$.

NMR Spectroscopy. $[Mn(L)](ClO_4)_2$. The ^1H NMR spectrum in d_6-dmso solution at 300 K showed only two very broad peaks at δ_H 50 (fwhh: 6000 Hz) and −10

(31) Casanova, D.; Cirera, J.; Llunell, M.; Alemany, P.; Avnir, D.; Alvarez, S. *J. Am. Chem. Soc.* **2004**, *126*, 1755–1763.
(32) Pinsky, M.; Avnir, D. *Inorg. Chem.* **1998**, *37*, 5575–5582.
(33) For iron(II) complexes, intense color changes from pale yellow−orange to deep red−purple typically accompany a spin transition from high-spin (S = 2) to low-spin (S = 0) states; for example, see: Gütlich, P. *Struct. Bonding* **1981**, *44*, 83–195.
(34) Bencini, A.; Bianchi, A.; Dapporto, P.; Garcia-Espana, E.; Marcelino, V.; Micheloni, M.; Paoletti, P.; Paoli, P. *Inorg. Chem.* **1990**, *29*, 1716–18.
(35) Matzapetakis, M.; Karligiano, N.; Bino, A.; Dakanali, M.; Raptopoulou, C. P.; Tangoulis, V.; Terzis, A.; Giapintzakis, J.; Salifoglou, A. *Inorg. Chem.* **2000**, *39*, 4044–4051.

(fwhh: 3000 Hz). These peaks shift and sharpen at higher temperatures. At 430 K, the peaks are observed at δ_H 30 (fwhh: 4500 Hz) and −4 (fwhh: 2000 Hz). As the spectra are largely uninformative, no further NMR investigation was undertaken.

[Fe(L)](ClO$_4$)$_2$. The ^{1}H NMR spectra of [Fe(L)](ClO$_4$)$_2$ display paramagnetically shifted peaks in the range δ_H +150 to −60, see for example, Figure 3, as is typical for high-spin iron(II) centers.[17−30,34−44] On warming above room temperature, pairs of peaks in the spectra coalesce, indicative of a fluxional/exchange process. To assign the spectra and to fully characterize the underlying exchange process, [Fe(L)](ClO$_4$)$_2$ was subjected to detailed NMR experiments. The following spectra were acquired: ^{1}H NMR spectra of the complex in d_6-dmso over the temperature range 298−440 K, in CD_2Cl_2 over the temperature range 190−300 K, and in CD_3OD over the temperature range 210−325 K; ^{1}H−^{1}H correlation spectroscopy (COSY), ^{1}H−^{1}H total correlation spectroscopy (TOSCY), ^{1}H−^{1}H nuclear Overhauser effect spectroscopy/exchange spectroscopy (NOESY/EXSY), and ^{1}H−^{13}C heteronuclear multiple-quantum coherence (HMQC) spectra in d_6-dmso at 410 K (high-temperature limit) and in CD_3OD at 268 K (low-temperature limit); a series of ^{1}H−^{1}H EXSY spectra at five temperatures between 311.9 and 250.5 K in CD_2Cl_2 to allow extraction of thermodynamic parameters. ^{1}H T_1 relaxation times were measured at 298 K in d_6-dmso and in CD_3OD.

Assignment of the ^{1}H NMR Spectra. Comparison of the ^{1}H NMR spectra, Figure 3 and Figures S4−S6 (Supporting Information), in the three solvents employed reveals common features and coalescences, indicative of the same species and behavior in all media. Plots of the chemical shift values of the peaks in d_6-dmso, CD_2Cl_2, and CD_3OD against the inverse of the temperature are linear, revealing typical Curie behavior, Figures S7−S9 (Supporting Information). As the temperature is decreased, the chemical shift range increases. In d_6-dmso, the temperature dependence of the highest-frequency peaks, assigned as CH_2 proton peaks (see below), differs from those of the other peaks, in that it has a steeper, less-linear slope. This difference has been previously observed for the α protons in the six-coordinate iron(II) complex [Fe(tpma)(SO$_3$CF$_3$)$_2$] (tpma = tris(2-pyridylmethyl)amine),[42] in which case it was attributed to the proximity of the α-pyridyl protons to the magnetically anisotropic $S = 2$ iron(II) center. The crossing of, and the discontinuities in, the lines in the CD_2Cl_2 and CD_3OD plots arise because peaks disappear

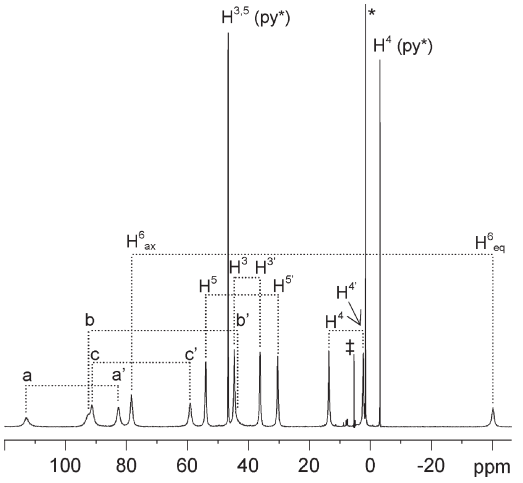

Figure 3. The 600 MHz ^{1}H NMR spectrum of [Fe(L)](ClO$_4$)$_2$ in CD_2Cl_2 at 297 K. Pairs of peaks for exchanging protons are indicated by the labels atop connecting horizontal lines. Methylene protons are labeled a−c, and the pyridyl protons are labeled according to ring position (e.g., H^4 and H$^{4\prime}$) with those of the central pyridyl indicated as "py*". (‡) Residual protio-solvent peak. (*) Water.

or (de)coalesce due to the intramolecular exchange process (see below).

The peaks in the ^{1}H NMR spectra were assigned using a combination of techniques:

1. Chemical Shift and Line Width Data. The magnitude of the paramagnetic shift of a proton peak is made up of two components, the electron−nucleus dipolar interaction and the Fermi contact shift. The Fermi contact shift is generally much larger; the electron−nucleus dipolar interaction is proportional to $(3\cos^2\theta - 1)/r^3$, where θ is the angle between the principal axis of the (magnetic susceptibility anisotropy tensor of the) complex and the iron-ion-to-proton internuclear vector and r is the internuclear distance between the proton and the iron ion.[37,38] The peak linewidths in paramagnetic systems are also determined by dipolar and contact contributions. The former is proportional to $1/r^6$, while the latter depends on the square of the hyperfine coupling constant, which in turn scales with the contact shift.[37,38] Thus, broader peaks at the highest or lowest frequency should arise from the protons closest to the paramagnetic center. Table S2 (Supporting Information) presents average iron-to-proton distance data for [Fe(L)]$^{2+}$.
2. T_1 Relaxation Times. Protons closer to the paramagnetic iron center will relax faster than those more distant. The T_1 values range from ∼0.1 to ∼18 ms at 298 K, Tables S1 and S2 (Supporting Information), and are typical of paramagnetic iron(II) complexes.[24,40,43] The relaxation times in CD_3OD are shorter than those in d_6-dmso, which is unexpected, since the relative solvent viscosity at 298 K of methanol (0.544 mPa) is less than that of dimethylsulfoxide (1.987 mPa). A plausible explanation for this is that the molecule's correlation time, in dmso at least, is sufficiently long for it to be greater than the correlation time corresponding to the minimum in the T_1 versus correlation time curve, so that increasing viscosity leads to an increase in T_1.
3. Integral Values. For example, in the d_6-dmso spectrum at 298 K, the peak at δ_H −1.3 has the lowest

(36) Solomon, E. I.; Brunold, T. C.; Davis, M. I.; Kemsley, J. N.; Lee, S. K.; Lehnert, N.; Neese, F.; Skulan, A. J.; Yang, Y. S.; Zhou, J. *Chem. Rev.* **2000**, *100*, 235–349.
(37) La Mar, G. N.; Horrocks, W. D., Jr.; Holm, R. H. *NMR of Paramagnetic Molecules, Principles and Applications*; Academic Press: New York, 1973.
(38) Bertini, I. *Coord. Chem. Rev.* **1996**, *150*, 1–292.
(39) Ming, L. J.; Jang, H. G.; Que, L.Jr. *Inorg. Chem.* **1992**, *31*, 359–64.
(40) Menage, S.; Zang, Y.; Hendrich, M. P.; Que, L.Jr. *J. Am. Chem. Soc.* **1992**, *114*, 7786–92.
(41) Blakesley, D. W.; Payne, S. C.; Hagen, K. S. *Inorg. Chem.* **2000**, *39*, 1979–1989.
(42) Diebold, A.; Hagen, K. S. *Inorg. Chem.* **1998**, *37*, 215–223.
(43) Mandon, D.; Machkour, A.; Goetz, S.; Welter, R. *Inorg. Chem.* **2002**, *41*, 5364–5372.
(44) Machkour, A.; Mandon, D.; Lachkar, M.; Welter, R. *Inorg. Chim. Acta* **2005**, *358*, 839–843.

integrated intensity. If this peak is assigned a relative integral of 1, then the overall sum of the relative integral values is 31, the total of protons in L. The H^4 proton on the central pyridyl (py*) ring is the only unique proton; thus, the δ_H −1.3 resonance is attributed to this proton.

4. Peak Coalescences. This can be illustrated by the four peaks at δ_H 57.3, 47.5, 38.5, and 32.0 in the CD_3OD spectrum at 280 K, each integrating for two protons. In d_6-dmso at all temperatures, these peaks have coalesced to give two peaks, each integrating as four protons. Thus, the four peaks must arise from two distinct sets of protons. This information, when coupled with the fact that the four peaks have some of the longest T_1 times and are thus probably some of the most distant protons from the iron center, suggests that the peaks arise from the four H^3 and four H^5 pyridyl protons. Previous assignments of the H^3 and H^5 pyridyl protons in related high-spin iron (II) complexes of pyridylalkylamine ligands support these assignments: for example, the H^3 and H^5 protons are assigned at δ_H 45.70 and 34.37 in $[Fe(tpaa)](ClO_4)_2$ (tpaa = tris(*N*-(2-pyridylmethyl)-2-aminoethyl)amine),[24] at δ_H 47.0 and 45.2 in $[Fe_2(tpma)_2(OAc)_2](BPh_4)_2$,[40] and at δ_H 41.75 (coincident) in $[Fe(tpma)_2](BPh_4)_2$.[42] We note that there is ambiguity in the assignment of H^3 and H^5, which may lead to their assignments being interchanged. This does not affect any of the discussion relating to the exchange process (see below).

5. $^1H-^{13}C$ Coupling Constants. All $^1H-^{13}C$ coupling constants and indirectly determined ^{13}C chemical shift values, from $^1H-^{13}C$ HMQC experiments that were run in d_6-dmso at 410 K and in CD_3OD at 268 K, are listed in Tables S4 and S5 (Supporting Information). The $^1H-^{13}C$ coupling constants for alkyl protons at ∼120−140 Hz are differentiated from those for pyridyl (aromatic) protons at > 160 Hz. The observed $^1H-^{13}C$ couplings are all greater than 170 Hz, thus allowing assignment of the peaks to pyridyl protons.

6. $^1H-^1H$ COSY and $^1H-^1H$ TOCSY Correlations. $^1H-^1H$ COSY and $^1H-^1H$ TOCSY experiments on the complex at 410 K in d_6-dmso were set up to reveal three bond correlations.[39] A summary of the cross-peak data is given in Table S4 (Supporting Information). Only the pyridyl protons are within three bonds of other protons, and therefore, the peaks at δ_H 37.1, 28.9, 28.6, and 7.3 and 2.4 are all from pyridyl protons. As the H^4(py*) peak at δ_H 2.4 (integrates for one proton) displays a three-bond correlation with the peak at δ_H 37.1 (integrates as two protons), the latter can be attributed to $H^{3,3'}$(py*). The peak at δ_H 7.3 correlates to both δ_H 28.9 and 28.6 in the COSY spectrum, consistent with it being due to H^4(py).

7. $^1H-^1H$ NOESY/EXSY Correlations. Cross-peaks in the $^1H-^1H$ NOESY/EXSY spectra, for example, Figure 4, reveal exchanging protons. Figure 3 shows the corresponding 1-D ^1H NMR spectrum with the pairs of exchanging protons indicated. From the $^1H-^1H$ NOESY experiment, the rate of exchange in CD_2Cl_2 at 297 K is 625 ± 50 s^{-1}.

The collective information from techniques 1−7 allows assignment of the ^1H NMR spectra, Table 2. The spectra

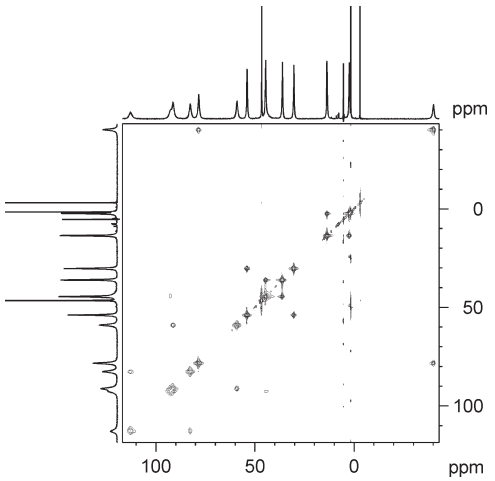

Figure 4. The 600 MHz $^1H-^1H$ EXSY NMR spectrum of $[Fe(L)](ClO_4)_2$ in CD_2Cl_2 at 297 K. The mixing time was 500 μs.

are fully consistent with a (pseudo)-C_2-symmetric, seven-coordinate structure for $[Fe(L)]^{2+}$ in which the two bpa domains are equivalent but the pyridylmethyl arms within each domain are inequivalent, adopting axial or equatorial positions (see also the description of the crystal structure above). Peaks ascribable to unbound pyridyl rings, which would appear as relatively sharp peaks in the diamagnetic region of the ^1H NMR spectra,[43] are never observed. The spectra, therefore, are inconsistent with lower coordinate species having dangling noncoordinated pyridylmethyl arms (that do not exchange with coordinated pyridylmethyl arms at least).

The Exchange Process. The following observations can be made about the exchange process in $[Fe(\kappa^7N\text{-L})](ClO_4)_2$:

1. In the ^1H NMR spectrum of $[Fe(\kappa^7N\text{-L})](ClO_4)_2$ and deliberately added excess free ligand in CD_3OD, separate peaks are observed for free L and the complex. This indicates that free ligand only exchanges with the bound ligand on a time scale slower than that of the NMR experiment. The observed exchange process is therefore intramolecular.
2. Equivalent pyridylmethyl arms in the NMR spectra at the high-temperature limit are observed.
3. There is a pairwise exchange of protons in the spectra. For example, Table 3 lists the pairs of peaks observed for the exchanging protons in the $^1H-^1H$ EXSY spectrum of $[Fe(L)](ClO_4)_2$ in CD_2Cl_2 at 297 K. Thus, C_2 symmetry is maintained by the exchange process, implying that the two bpa domains of L are equivalent.
4. The peaks corresponding to the central pyridyl protons (H^3(py*), H^4(py*), and H^5(py*)) remain (relatively) sharp at all temperatures, suggesting that this donor is not involved in the fluxional process.
5. There is an absence of peaks for a dangling, noncoordinated pyridylmethyl arm at all temperatures (see above).

In toto, these observations point to the exchange of the equatorial and axial pyridylmethyl arms of each bpa domain in seven-coordinate $[Fe(L)]^{2+}$ as the observed exchange process. Notably, the high-frequency peak, δ_H 78 (^1H NMR spectrum at 297 K, CD_2Cl_2), attributed to the two H^6 pyridyl protons undergoes exchange with the

Table 2. Proton Peak Chemical Shifts (±0.2 ppm) and Assignments for [Fe(L)]$(ClO_4)_2$ in CD_2Cl_2 at 297 K

assignment	chemical shift (ppm)
CH_2 (2H)	113.0
CH_2 (2H)	92.8
CH_2 (2H)	91.3
CH_2 (2H)	82.6
H^6_{ax} (py) (2H)	78.4
CH_2 (2H)	59.0
H^5(py) (2H)	53.9
$H^{3,5}$(py*) (2H)	46.6
H^3(py) (2H)	44.6
CH_2 (2H)	~44.0
H^3(py) (2H)	36.1
H^5(py) (2H)	30.3
H^4(py) (2H)	13.6
H^4(py) (2H)	2.3
H^4(py*) (1H)	−3.1
H^6_{eq} (py) (2H)	−40.2

lowest-frequency peak at δ_H −40. Since the magnitude of the dipolar interaction component of the paramagnetic shift (pseudocontact shift) of a proton signal is proportional to $(3\cos^2\theta - 1)/r^3$ and all of the pyridyl donors are all bound to the iron(II) ion, the distance r will be nearly invariant, implying that the angle θ for the two sets of exchanging H^6 pyridyl protons must vary considerably. Thus, the observed chemical shifts are consistent with axial (θ = ~0°, $(3\cos^2 0 - 1) = +2$) to equatorial (θ = ~90°, $(3\cos^2 90 - 1) = -1$) exchange of H^6(py). Caution should be exercized with this interpretation, however, since the Fermi contact component of the paramagnetic shift (contact shift) is normally dominant and may have opposite signs in the two different H^6 environments.

Thermodynamic parameters for the exchange rate of the axial and equatorial arms for $[Fe(L)]^{2+}$ in CD_2Cl_2 have been obtained. Variable-temperature 600 MHz $^1H-^1H$ NOESY/EXSY experiments were used to obtain the exchange rates at different temperatures. An Arrhenius plot, Figure 5, affords $\Delta H^{\ddagger} = 53.6 \pm 2.8$ kJ mol^{-1}, $\Delta S^{\ddagger} = -10.0 \pm 9.7$ J K^{-1} mol^{-1}, and $\Delta G^{\ddagger}$ (298 K) = 50.6 kJ mol^{-1}.

DFT Calculations and the Mechanism of Exchange. Comparison with the thermodynamic parameters for the associative exchange of the one dangling and two equatorially bound pyridylmethyl arms in the ruthenium congener $[Ru(\kappa^6N\text{-L})]^{2+}$ [$\Delta H^{\ddagger} = 56 \pm 1$ kJ mol^{-1} and $\Delta S^{\ddagger} = -10 \pm 3$ J K^{-1} mol^{1}; $\Delta G^{\ddagger}$ (298 K) = 53 kJ mol^{-1}][28] is informative. In this octahedral ruthenium(II) complex, exchange of the pyridylmethyl arms between axial and equatorial coordination modes is not observed: the "middle pyridine (py*) and the two axial pyridylmethyl arms form rigid non-exchanging bonds".[28] That the iron (II) complex is seven-coordinate whereas its ruthenium (II) congener is six-coordinate is readily reconciled by simple ligand-field considerations. The ligand field for the iron(II) species is comparatively weak. Thus, the complex is high-spin ($S = 2$) with no electronic preference for geometry and seven-coordination, which minimizes geometric distortion, is favored, whereas the much larger ligand field for the ruthenium(II) ion leads to a low-spin d^6 ($S = 0$) complex and, consequently, a strong preference for an octahedral, albeit strained and severely distorted, geometry. The negative $\Delta S^{\ddagger}$ value for the exchange in the ruthenium complex is consistent with an associative process through a seven-coordinate intermediate,[28] and the $\Delta S^{\ddagger}$ value for the iron complex has a large error associated with it and may be consistent with a more strained, rigid transition state.

Table 3. Exchanging Pairs of Protons in the $^1H-^1H$ EXSY Spectrum of [Fe(L)]$(ClO_4)_2$ in CD_2Cl_2 at 297 K[a]

Assignment	^1H chemical shifts (ppm)
CH_2 (4H)	113.0 ↔ 82.6
CH_2 (4H)	92.8 ↔ ~44.0
CH_2 (4H)	91.3 ↔ 59.0
H^6(py) (4H)	78.4 ↔ −40.2
H^5(py) (4H)	53.9 ↔ 30.3
$H^{3,5}$(py*) (2H)	46.6[b]
H^3(py) (4H)	44.6 ↔ 36.1
H^4(py) (4H)	13.6 ↔ 2.3
H^4(py*) (1H)	−3.1[b]

[a] The ↔ denotes pairs of signals displaying cross-peaks in the exchange spectrum. [b] denotes protons that do not undergo exchange.

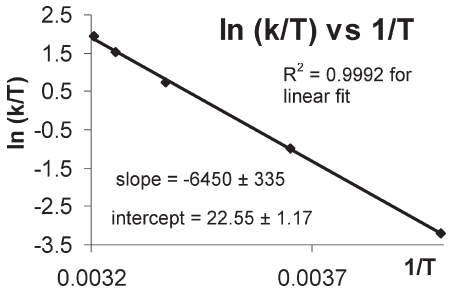

Figure 5. An Arrhenius plot for the exchange of isomers of [Fe(L)]$(ClO_4)_2$ in CD_2Cl_2. See Table S6 (Supporting Infomation) for details.

The ground state and possible intermediate/transition states for the exchange process in $[Fe(\kappa^7N\text{-L})]^{2+}$ were explored by DFT calculations using the hybrid UB3LYP functional[45,46] (see Experimental Section and Supporting Information). Geometry minimizations for the ground-state complex converge to afford a seven-coordinate species, Figure 6a, with a geometry that closely mirrors that found in the crystal structure. This structure had the lowest energy of any structure calculated. Seven-coordination is slightly favored over a six-coordinate species with a dangling pyridylmethyl arm (such as found for ground-state $[Ru(\kappa^6N\text{-L})]^{2+}$; e.g., see Figure 6b) by 9−40 kJ mol^{-1}, a small, but nevertheless, significant energy difference. While a complete search of conformational space for the six-coordinate isomers was impractical, several isomers were generated and their geometries optimized. The initial geometries were generated by starting with the lowest-energy seven-coordinate structure then rearranging either an equatorial or axial pyridyl arm so that they were removed from the direct coordination sphere of the iron center. The lowest-energy six-coordinate structures obtained were either 9 kJ mol^{-1} or 40 kJ mol^{-1} higher in energy when either an axially or equatorially bound arm was removed from coordination, respectively.

The first possible exchange mechanism investigated was synchronous rotation of the two pyridylmethyl arms of

(45) Becke, A. D. *J. Chem. Phys.* **1993**, *98*, 5648–5652.
(46) Lee, C. T.; Yang, W. T.; Parr, R. G. *Phys. Rev. B* **1988**, *37*, 785–789.

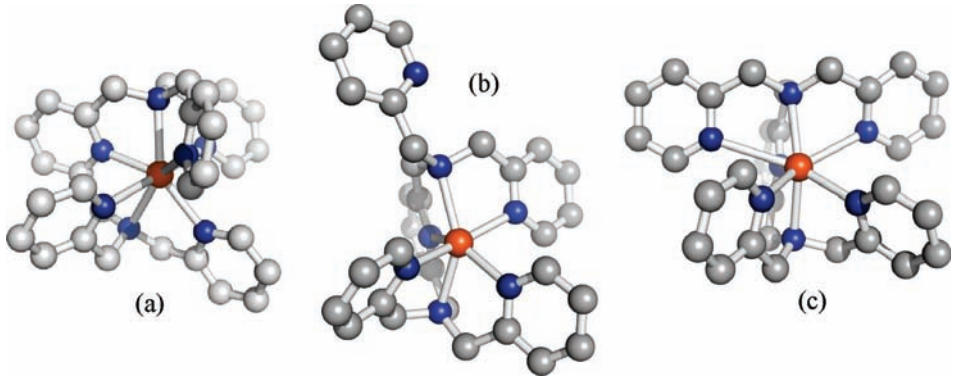

Figure 6. Calculated structures [and relative energies] for the (a) ground [0 kJ mol^{-1}], (b) intermediate [37.5 kJ mol^{-1}], and (c) transition [53.5 kJ mol^{-1}] structures for the exchange mechanism portrayed in Scheme 2. UB3LYP/6-311+G*(Fe), 6-31G*(C, H, N).

each bpa domain through a distorted edge-capped prismatic (C_{2v}) intermediate or transition state, the mechanism depicted diagramatically in Scheme 1. Conceptually, this process is the pentagonal bipyramidal equivalent of the more well-known turnstile rotation mechanism found in trigonal bipyramidal systems. A minimum-energy structure constrained to a seven-coordinate C_{2v} geometry was found to be 256 kJ mol^{-1} higher in energy than the C_2 ground state and corresponded to a high-order saddle point on the energy surface and not a transition structure. Severe inter-ring clashes between pyridyls PY^1−PY^4 always destabilize a C_{2v} transition state to the point where it lies at an unobtainably high energy.

Dissociation of one (or more) pyridylmethyl arm(s) to give a six- (or lower) coordinate intermediate followed by rearrangement and rebinding of the arm(s) was investigated next. The absence of signals for intermediate species in the NMR spectra implies that any such intermediate(s) must be short-lived or rapidly exchanging with the seven-coordinate structure if present in significant quantities and so not observed. In the latter case, the observed NMR parameters would therefore represent a population weighted average of the six- and seven-coordinate isomers available, the population weighting in turn being dependent on the relative free energies of these isomers. For $[Ru(L)]^{2+}$, binding of the dangling pyridylmethyl arm in an equatorial position affords a pentagonal bipyramidal intermediate from which a loss of the other equatorially bound pyridylmethyl arm leads to dangling equatorial arm exchange and simultaneously exchanges the environments of the two axial pyridylmethyl arms. The two sets of pyridylmethyl arms, comprising the two axial arms and the dangling and equatorial arms, are always inequivalent. Thus, the mechanism of exchange in $[Fe(L)]^{2+}$ is more complex than the inverse (dissociation and rebinding of pyridylmethyl arms) of that for $[Ru(L)]^{2+}$.

Scheme 2 shows a plausible mechanism that would exchange all pyridylmethyl arms in $[Fe(L)]^{2+}$. DFT calculations reveal the energy−structure landscape for the complex ion to be relatively flat, with dissociation of an *equatorial* pyridylmethyl arm producing distorted octahedral intermediate species (see Figure 6b), as already mentioned, only 37.5 kJ mol^{-1} above the ground state. If the dangling pyridylmethyl arm rebinds "below" the adjacent axial arm, nearer the central pyridyl, as illustrated in Scheme 2, a transition structure with C_s geometry can be envisaged in which the two pyridylmethyl arms of each bpa domain are equivalent (as is required for an exchange process that averages the environments of all arms). A geometry optimization wherein the system is constrained to a C_s structure like the transition state shown in Scheme 2 produces a structure that is only 56 kJ mol^{-1} higher in energy than the seven-coordinate C_2 ground state, comparable to the observed activation enthalpy. However, vibrational analysis shows that the C_s structure is a second-order saddle point and not a transition structure. A search for a nearby transition structure without symmetry constraints successfully found a closely related seven-coordinate C_1 structure, which is shown in Figure 6c. The reason that the transition structure lacks C_s symmetry is that the central pyridyl ring containing N4 prefers to be not coplanar with the equatorial plane—this can also be seen in the X-ray structure. The central ring must change the direction of twisting in a separate step in order to fully interchange the two pyridyl arms attached to the same sp^3 nitrogen. This will be a low-energy process relative to the energy required to reach the C_1 transition structure. The normal coordinate analysis of the optimized C_1 transition structure reveals one imaginary frequency indicative for a saddle point on the energy hypersurface. The energy difference between the optimized ground and C_1 transition states is 53.5 kJ mol^{-1}, which compares very favorably with the experimentally found 53.6 ± 2.8 kJ mol^{-1}.

In modeling the pathway shown in Scheme 2 with relaxed potential energy surface scans, no structures higher in energy than the transition structure were located; that is, the barriers to conversion between the six-coordinate and seven-coordinate structures are lower than the energy of the transition structure for the ligand exchange process.

When entropy is also accounted for, the DFT calculations predict that the six-coordinate complex in which one of the *axial* pyridyl arms has been removed from the coordination sphere of the metal has a free energy, ΔG, that is only 1.5 kJ mol^{-1} higher in energy at 298 K than the seven-coordinate, X-ray-like, structure. This would imply that a significant fraction of the complex in this particular six-coordinate conformation (which is not involved in the exchange process) would be expected to exist in equilibrium with the seven-coordinate structure. As noted above, only one set of NMR resonances is observed even

Scheme 1

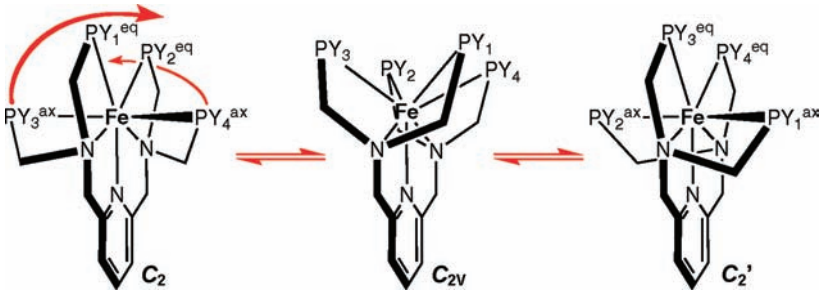

Scheme 2. A Plausible Mechanism for the Exchange of the Pyridylmethyl Arms

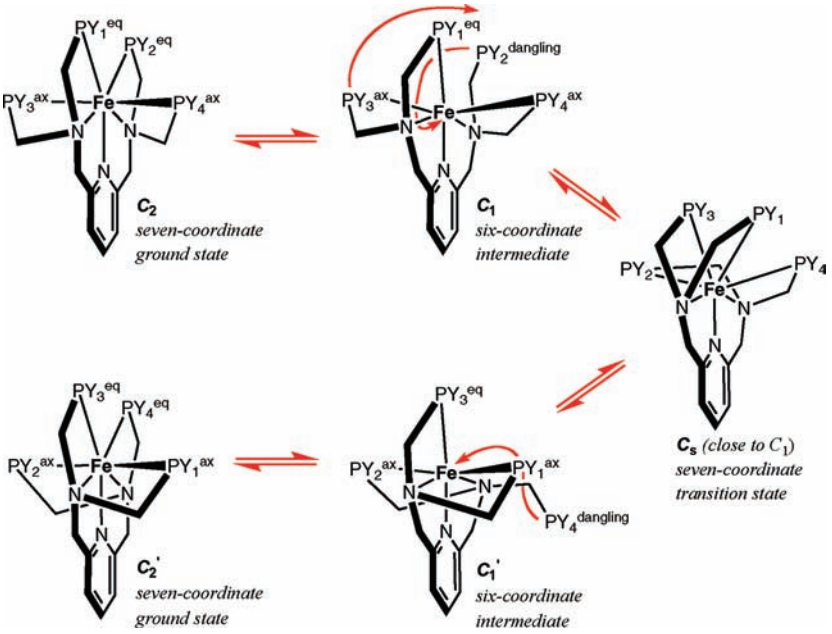

at the lowest temperatures used (190 K). This would mean that, if the six-coordinate complex is also present, it must be in fast exchange with the seven-coordinate complex at all temperatures, and therefore the barrier to their interconversion must be low.

A relaxed potential energy surface calculation was performed starting from the minimum energy, seven-coordinate structure, in which the axial Fe−N5 distance was increased from a starting value of 2.47 Å up to a value of 5.07 Å in 0.2 Å steps. The maximum energy on this path was found to be 34 kJ mol^{-1} above the energy of the seven-coordinate ground state when the Fe−N5 distance was 4.47 Å. This models the process of (reversible) uncoordination of one of the *axial* pyridyl ligands and its movement out of the coordination sphere of the iron. An approximate energy barrier of 34 kJ mol^{-1} (which does not account for zero point energy or entropy) is sufficiently low so that it is plausible that there is an equilibrium concentration of the six-coordinate complex in the presence of a dominant seven-coordinate isomer and that these two are interchanging sufficiently rapidly so that the interchange process remains undetectable in the NMR spectra at low temperatures. We note also that a low equilibrium concentration of the six-coordinate species may explain the weak band at 1160 nm in the UV−vis−NIR spectrum.

Conclusion

Tetrakis(2-pyridylmethyl)-2,6-bis(aminomethyl)pyridine (L) forms seven-coordinate complexes with high-spin manganese(II) and iron(II) ions, as these are comparatively large with no electronically driven geometric preference. The iron (II) ($S = 2$) complex ion, $[Fe(\kappa^7N\text{-L})]^{2+}$, is ammenable to study by paramagnetic NMR spectroscopy, and this work demonstrates that a full array of 1D and 2D (e.g., $^1H-^1H$ COSY, $^1H-^1H$ TOSCY, $^1H-^1H$ NOESY/EXSY, and $^1H-^{13}C$ HMQC) NMR techniques may be employed. The ^1H NMR spectrum has been assigned, and the axial and equatorial pyridylmethyl arms are revealed to undergo exchange with $\Delta H^{\ddagger} = 53.6 \pm 2.8$ kJ mol^1 and $\Delta S^{\ddagger} = -10.0 \pm 9.7$ J K^{-1} mol^{-1}. The process exchanges the enantiomers of the seven-coordinate complex ion. DFT calculations have been used to explore possible exchange pathways. Synchronous rotation of both bpa domains through an edge-capped prismatic (C_{2v}) intermediate is discounted by a high-energy barrier that arises from interpyridine ring clashes. Rather, an excellent match is found between the experimental energy barrier and that calculated for an exchange pathway that passes through a seven-coordinate intermediate which is slightly distorted from C_s symmetry formed by dissociation and rebinding of an equatorial pyridylmethyl arm, as depicted in Scheme 2.

Table 4. Crystallographic Data for $[M(L)](ClO_4)_2$ (M = Mn, Fe)

	$[Mn(L)](ClO_4)_2$	$[Fe(L)](ClO_4)_2$
empirical formula	$C_{31}H_{31}Cl_2MnN_7O_8$	$C_{31}H_{31}Cl_2FeN_7O_8$
fw	755.5	756.4
T, K	294	294
λ, Å	0.71073	0.71073
cryst syst	triclinic	triclinic
space group	$P\bar{1}$	$P\bar{1}$
a, Å	11.480(6)	11.409(6)
b, Å	12.232(7)	12.660(6)
c, Å	14.203(8)	13.691(8)
α, deg	111.36(3)	71.41(3)
β, deg	97.77(3)	67.61(3)
γ, deg	111.22(3)	70.58(3)
V, Å^3	1648(2)	1682(1)
Z	2	2
D_c, g/cm^3	1.52	1.49
μ (Mo Kα), mm^{-1}	0.620	0.665
cryst size (mm)	irregular	$0.30 \times 0.12 \times 0.07$
θ, deg		25
h range	−12 to +12	0 to 13
k range	−13 to +12	−15 to +15
l range	0 to 15	−16 to +16
reflns collected	4299	5917
unique reflns > threshold	3347 ($I > 2\sigma I$)	4001 ($I > 2\sigma I$)
no. params	196	189
goodness-of-fit	1.79	1.65
R1	0.051	0.058
wR2	0.077	0.075
weighting scheme	$w = 1/[\sigma^2(F) + 0.0016F^2]$	$w = 1/[\sigma^2(F) + 0.004F^2]$
largest diff. peak and hole, e·Å^{-3}	+0.64 and −0.48	+0.91 and −1.16

Experimental Section

Materials and General Methods. Tetrakis(2-pyridylmethyl)-2,6-bis(aminomethyl)pyridine (L) was prepared using our previously published method.[29,30] All other chemicals were purchased from Aldrich and used without further purification. ^{1}H and ^{13}C{^{1}H} NMR spectra were recorded on Bruker AC 300F (300 MHz), Bruker DPX 300 (300 MHz), or DMX 600 (600 MHz) spectrometers. Each temperature recorded during variable-temperature exchange rate measurement experiments was calibrated with a K-type thermocouple in a 5 mm NMR tube filled to a normal depth with methanol. The thermocouple was placed into the center point of the temperature-equilibrated probe immediately before or after each spectrum was acquired. Elemental analyses for C, H, and N were carried out at either the Australian National University Microanalytical Laboratory or at the Campbell Microanalytical Laboratory, University of Otago, New Zealand. Prior to being sent for analysis, samples were dried at 40 °C for 48 h under a vacuum (0.2 mmHg) over phosphorus pentoxide. X-Band EPR spectra were recorded on a Bruker EMX 10 spectrometer ($\nu \approx 9.5$ GHz). Spectra were obtained at 77 K using a liquid-nitrogen-filled low-temperature EPR dewar. For solution spectra, the sample concentration was $\sim 1 \times 10^{-3}$ M. Infrared spectra were recorded as KBr discs using a Mattson Genesis series FTIR spectrometer (1.0 cm^{-1} resolution), and electronic absorption spectra were recorded on a CARY 5 spectrometer in the dual-beam mode. Electrochemical measurements were recorded using a Pine Instrument Co. computer-controlled bipotentiostat using a standard three-electrode cell, as previously described in detail.[47] Data are referenced to the ferrocenium−ferrocene couple, which was measured in situ as an internal standard.

Preparations. ***Caution!*** *Although no problems were encountered in this work, perchlorate salts of metal ions bound by oxidizable organic ligands are potentially explosive and should be handled taking appropriate precautions.*

$[Mn(L)](ClO_4)_2$. L (51 mg, 0.10 mmol) was dissolved in methanol (5 mL), and $Mn(ClO_4)_2 \cdot 6H_2O$ (75 mg, 0.20 mmol) in ethanol (2 mL) was added followed by $LiClO_4$ (71 mg, 0.44 mmol) in water (1 mL). This was left to evaporate. Clear crystalline blocks of the product formed (57 mg, 74%). Elem anal. found: C, 49.08; H, 4.12; N, 12.99%. $MnC_{31}H_{31}N_7Cl_2O_8$ requires: C, 49.29; H, 4.14; N, 12.98%). ESI-MS m/z (%): 655 (30) $\{[Mn(L)] + (ClO_4)\}^+$, 278 (100) $[Mn(L)]^{2+}$. IR ν_{max}/cm^{-1} (KBr): 3430s (OH), 1602s (py), 1571m (py), 1480m (py), 1087s (ClO_4), 768m (py), 735w. λ_{max}/nm: (CH_2Cl_2) 290 (ε/dm^3 mol^{-1} cm^{-1} 3600), 320 (3600); (CH_3CN) 290 (3850), 320 (3800); (dmf) 290 (3900), 320 (3800); no other peaks with $\varepsilon > 1$. Λ_M/S cm^2 mol^{-1}: (CH_3CN) 276; (dmf) 122.

$[Fe(L)](ClO_4)_2$. $Fe(ClO_4)_2 \cdot 2H_2O$ (52 mg, 0.20 mmol) and L (101 mg, 0.20 mmol) were combined in ethanol (5 mL) to give a red−brown precipitate, which was further recrystallized from methanol−water (4:1) to afford the yellow crystalline product (55 mg, 36%). Elem anal. found: C, 48.47; H, 4.09; N, 12.73%. $FeC_{31}H_{31}N_7Cl_2O_8 \cdot 4H_2O$ requires: C, 48.08; H, 4.26; N, 12.67%). ESI-MS m/z (%): 656 (20) $\{[Fe(L)] + (ClO_4)\}^+$, 279 (100) $[Fe(L)]^{2+}$. IR ν_{max}/cm^{-1} (KBr): 3443s (OH), 1601s (py), 1570m (py), 1477m (py), 1082s (ClO_4), 765m (py), 735w. λ_{max}/nm (CH_2Cl_2) 290 (ε/dm^3 mol^{-1} cm^{-1} 3900), 320 (3800), 389 (1090), 1165 (10); (CH_3CN) 290 (3900), 320 (3800), 389 (1090), 1160 (10); (dmf) 290 (3850), 320 (3850), 388 (1080), 1157 (10); (CH_3NO_2) 390 (1075), 1165 (10); (KBr disk) 400. Λ_M/S cm^2 mol^{-1}: (CH_3CN) 338; (dmf) 103.

Quantum Chemical Calculations. Calculations were performed using the Gaussian 03 (rev. E) software package[48] running on dual-/quad-core Linux workstations. All reported DFT calculations were performed using unrestricted open-shell wave functions, the B3LYP functional (UB3LYP),[45,46] and the spin multiplicity of the high-spin iron (II) complexes set to five (quintet). The basis set employed consisted of the Gaussian 03 implementation of the 6-311+G* basis set for the iron atoms and the 6-31G* basis set for all other elements. Some structures were geometrically preoptimized using the PCGAMESS package[49] with the equivalent functional and basis set combination prior to being optimized using Gaussian. All minimum-energy structures were calculated without any symmetry constraints and were confirmed to be minima by calculating their normal vibrations within the harmonic approximation and observing that there were no imaginary frequencies. Energies quoted include correction for zero-point vibrational energy. Calculations employed the "tight" optimization and SCF convergence criteria (except for the relaxed potential energy surface scans,

(47) He, Z. C.; Colbran, S. B.; Craig, D. C. *Chem. Eur. J.* **2003**, *9*, 116–129.

(48) Frisch, M. J.; Trucks, G. W.; Schlegel, H. B.; Scuseria, G. E.; Robb, M. A.; Cheeseman, J. R.; Montgomery, J. A., Jr.; Vreven, T.; Kudin, K. N.; Burant, J. C.; Millam, J. M.; Iyengar, S. S.; Tomasi, J.; Barone, V.; Mennucci, B.; Cossi, M.; Scalmani, G.; Rega, N.; Petersson, G. A.; Nakatsuji, H.; Hada, M.; Ehara, M.; Toyota, K.; Fukuda, R.; Hasegawa, J.; Ishida, M.; Nakajima, T.; Honda, Y.; Kitao, O.; Nakai, H.; Klene, M.; Li, X.; Knox, J. E.; Hratchian, H. P.; Cross, J. B.; Bakken, V.; Adamo, C.; Jaramillo, J.; Gomperts, R.; Stratmann, R. E.; Yazyev, O.; Austin, A. J.; Cammi, R.; Pomelli, C.; Ochterski, J. W.; Ayala, P. Y.; Morokuma, K.; Voth, G. A.; Salvador, P.; Dannenberg, J. J.; Zakrzewski, V. G.; Dapprich, S.; Daniels, A. D.; Strain, M. C.; Farkas, O.; Malick, D. K.; Rabuck, A. D.; Raghavachari, K.; Foresman, J. B.; Ortiz, J. V.; Cui, Q.; Baboul, A. G.; Clifford, S.; Cioslowski, J.; Stefanov, B. B.; Liu, G.; Liashenko, A.; Piskorz, P.; Komaromi, I.; Martin, R. L.; Fox, D. J.; Keith, T.; Al-Laham, M. A.; Peng, C. Y.; Nanayakkara, A.; Challacombe, M.; Gill, P. M. W.; Johnson, B.; Chen, W.; Wong, M. W.; Gonzalez, C.; Pople, J. A. *Gaussian 03*, revision E.01; Gaussian, Inc.: Wallingford, CT, 2004.

(49) Granovsky, A. A. *PC GAMESS*, version 7.0. http://classic.chem.msu.su/gran/gamess/index.html (accessed Apr 2009).

which employed the normal criteria) and the "ultrafine" grid for all calculations, as implemented in the Gaussian 03 software. To optimize the probability that electronic ground states had been calculated, key optimized structures (see Supporting Information Table 1S, A−H) were examined with the "stable" keyword to ensure that lower-energy wave functions were not available. All calculations were performed on molecules in a vacuum. Graphics were generated using the Pymol software package.[50]

X-Ray Crystallography. Relevant crystal, data collection, and refinement data for the X-ray crystal structures of $[M(L)](ClO_4)_2$ (M = Mn, Fe) are summarized in Table 4. Full details and data (excluding structure factors) in CIF format are available in the Supporting Information.

Acknowledgment. We thank Prof. Stuart MacGregor for helpful discussions and the Australian Research Council (Grant: DP0557462) and UNSW for funding. We also thank a referee for suggesting the use of continuous shape measures for analysis of coordination geometry.

Supporting Information Available: Crystallographic data (CIF format) and additional figures of the $[Fe(L)]^{2+}$ complex ion, figures of UV−vis−NIR and variable-temperature NMR spectra, details of DFT calculations, and Cartesian coordinates and drawings of stationary points for all located structures. This material is available free of charge via the Internet at http://pubs.acs.org.

(50) DeLano, W. L. *The PyMOL Molecular Graphics System* (2002). http://www.pymol.org (accessed Apr 2009).